RNi$_2$B$_2$C (R = Ho, Dy, Tb and Pr) single crystals grown by the cold copper crucible method

A Durán†, E Muñoz†, S Bernès†‡ and R Escudero†

† Instituto de Investigaciones en Materiales, Universidad Nacional Autónoma de México, Apartado Postal 70-360, México DF 04510, Mexico
‡ Facultad de Química, Universidad Nacional Autónoma de México, México DF 04510, Mexico

Abstract. Single crystals of RNi$_2$B$_2$C (R = Ho, Dy, Tb, Pr) have been grown on cold copper crucibles in a high-frequency induction furnace. As a result, shiny metallic and brittle platelike single crystals were obtained. They were examined by x-ray and scanning electron microscopy with WDX/EDX for local composition analysis and show a very good crystallographic structure and compositions. Resistivity and dc magnetic measurements were performed to study superconducting and magnetic properties. Besides known electronic properties of the RNi$_2$B$_2$C family, we report for the first time results for PrNi$_2$B$_2$C single crystals successfully obtained by this technique.

1. Introduction

The discovery of a new family of intermetallic superconductors in 1993 [1] created a new path in the search for novel superconductors. Coexistence of superconductivity and magnetism has been found in these materials [2, 3], whose magnetic ordering temperatures are much higher than those observed in rare earth rhodium borides and Chevrel phases [4, 5]. A large number of studies on the crystal structure and other physical properties have been carried out in the family of intermetallic alloys RT$_2$B$_2$C (R = Sc, Y, rare earth, Th, U; T = Ni, Rh, Pd, Ir, Pt) in polycrystalline samples. These materials crystallize in a filled variation of the well known ThCr$_2$Si$_2$ type tetragonal structure, with the C atoms in the rare earth planes and Ni$_2$B$_2$ layers separated by planes of R–C [6–9]. Some exhibit high superconducting transition temperatures, as compared with A-15 intermetallic alloys. In particular, much attention has been paid to the compound with a combination of Y–Pd–B–C [10] because it shows superconductivity at a high temperature record of 23 K, a temperature equal to the previous long-standing record for Nb$_3$Ge. However, not much is known about the interplay between superconductivity and magnetic behaviour in this borocarbide family. Magnetism in these systems plays a relevant role still not very well understood since in some cases it drives superconductivity and in others not. This is an area of study that requires more investigation.

From the viewpoint of the synthesis of the polycrystalline quaternary systems, these have been generally prepared by arc melting in a water-cooled copper hearth and subsequently annealed under an argon atmosphere [2, 7]. This method produces losses of light elements (boron and carbon) since the arc-heating temperature can be very high and difficult to control. As a consequence, the resulting composition is non-homogeneous due to lack of stoichiometry. Preliminary metallurgical studies have indicated that these compounds melt incongruently and for this reason it is very difficult to grow single crystals using the melt-growth method [11].

Nevertheless, single crystals of the quaternary borocarbides have been obtained by using a solution-growth method [12–15]. One of the problems with this method is the separation of the crystals from the solvent. Moreover, it has the inconvenience that for the same solvent not all compounds can be grown since the melting temperature is different for the different rare earths. However, bulk in YNi_2B_2C single-crystal form was recently obtained by floating-zone melting [16, 17]. Composition fluctuation, segregation at the melt–crystal interface and its tendency to cellular instability are the main factors that affect the growth process and the crystallographic perfection. Among the electronic properties studied, resistivity measurements display transition widths of the order $\Delta T_c = 0.7$ K, which may still indicate composition inhomogeneities in the superconducting phase. Preliminary studies in systems such as $HoNi_2B_2C$ and $DyNi_2B_2C$ suggest that slight changes in the stoichiometric composition (1:2:2:1) are detrimental to superconducting properties [18, 19]. These important facts have motivated us to look for another technique to grow single crystals. The aim of this paper is to show a new route of crystal growth for the intermetallic RNi_2B_2C (R = Ho, Tb, Dy and Pr) compounds with dimensions as large as several millimetres, using water-cooled copper boats, with a radio-frequency (RF) induction oven as the source of heating. Our studies indicate that we can produce $HoNi_2B_2C$, $DyNi_2B_2C$, $TbNi_2B_2C$ and $PrNi_2B_2C$ single crystals with almost exact stoichiometric composition. With this method boron and carbon losses can be maintained at minimum levels. The as-grown crystals with platelet-like form are several square millimetres in transversal area and with a thickness of the order of 0.02–0.3 mm. These platelets are encrusted in the melted buttons, which are about 2–3 g of the starting composition.

In this report we present a complete structural characterization, measurements of electrical resistance and magnetic susceptibility. These were carried out in order to confirm the single-crystalline nature of the RNi_2B_2C (R = Ho, Dy, Tb and Pr) compositions. We describe our findings for all four different rare earth single crystals. For the $PrNi_2B_2C$ composition we also investigate its transport and magnetic properties, since as far as we know there are no published measurements performed on single crystals for this composition.

2. Experimental details

2.1. Crystal growth

A high-frequency induction furnace (Stanelco type STA 30 kW) with 120 mm work coil as the heat source was used to produce the polycrystalline and single-crystal samples of the RNi_2B_2C (R = Ho, Dy, Tb, and Pr) compounds. The melting area is enclosed within a transparent chamber of silica glass tubing, mounted horizontally on a rigid main frame assembly. It is equipped with a mechanical or turbo pump to achieve high vacuum. A clean atmosphere was maintained with an argon flux. The starting material purities were ships and shots of lanthanide metals (99.9%), nickel powders -325 mesh (99.99%), boron lumps (99.8%) and carbon powder -100 mesh (99.9998%). These materials were weighed to obtain stoichiometric ratios of 1:2:2:1. In addition, nickel powders were pressed and used as susceptors for the RF power as precursors of the reaction. The starting composition was melted several times in order to improve the solubility of the components and achieve better homogenization of the button. At the end of the melting process the button is weighed again to check possible losses from the starting composition. After this homogenization the temperature of the polycrystalline sample is gradually increased for above ($\sim$50 K) to the melting point. This process takes about 30–45 minutes. In the molten zone one can distinguish convection currents on the surface of the button. At this stage the button is kept for 20–40 minutes at constant RF power to achieve equilibrium and to increase its homogeneity. After this procedure the RF power is

Table 1. Crystal data for single-crystal x-ray studies

| Empirical formula	CB_2Ni_2Pr	CB_2Ni_2Tb	CB_2Ni_2Dy	CB_2Ni_2Ho
Crystal size (mm^3)	$0.40 \times 0.15 \times 0.06$	$0.70 \times 0.30 \times 0.04$	$0.20 \times 0.20 \times 0.06$	$0.30 \times 0.20 \times 0.06$
Space group	*I4/mmm*	*I4/mmm*	*I4/mmm*	*I4/mmm*
a parameter (Å)	3.6996(2)	3.5521(2)	3.53800(10)	3.5109(2)
c parameter (Å)	9.9885(8)	10.4346(6)	10.5044(4)	10.5127(8)
Cell volume (Å^3)	136.713(15)	131.658(13)	131.488(7)	129.594(14)
2θ range ($^\circ$)	11.76–89.54	12.14–89.66	12.16–89.78	12.26–89.78
Reflections collected	1966	1872	1883	1841
Independent refl. (R_{int})[a]	200 (5.67%)	188 (6.44%)	190 (5.97%)	189 (8.31%)
$\langle I/\sigma(I)\rangle$ (all data)	31.19	39.21	28.74	27.99
Transmission factors	0.092–0.506	0.048–0.286	0.042–0.422	0.068–0.387
Data-to-parameter ratio	200/11	188/11	190/11	189/11
R_1, wR_2 (%)[a]	2.32, 5.58	2.32, 5.48	1.45, 2.60	3.35, 8.20
Goodness-of-fit S[a]	1.164	1.221	1.163	1.183

[a] $$R_{int} = \frac{\sum |F_0^2 - \langle F_0^2 \rangle|}{\sum F_0^2} \qquad R_1 = \frac{\sum ||F_0| - |F_c||}{\sum |F_0|} \qquad wR_2 = \sqrt{\frac{\sum w(F_0^2 - F_c^2)}{\sum w(F_0^2)^2}} \qquad S = \sqrt{\frac{\sum w(F_0^2 - F_c^2)^2}{m-n}}.$$

For R_{int}, both summations involve all input reflections for which more than one symmetry equivalent is averaged. R indices are calculated using all independent data. For S, m is the number of observed reflections and n is the number of parameters refined.

decreased in a steady slow ramp with speeds $\sim$5–7 K min^{-1}. Once the temperature is about 30–50 K below the melting point of the particular composition, the surface of the melt starts acquire a polycrystalline crust. The single crystals grow inside this crust with a platelet-like morphology and with 1:2:2:1 stoichiometry. The crystals are extracted in two forms: small platelike crystals are easily expulsed when the bulk button is broken; the dimension of these crystals in general are small, of the order $<1.3 \times <0.8 \times \sim 0.05$ mm^3. For large crystals without platelet-like shape, and dimensions about $4 \times 3 \times 0.5$ mm^3, they are separated from the bulk by cutting and removing the polycrystalline surface. We should mention that the mechanism of growth is similar to the skull melting technique used for growth complex oxides and binary compounds [20, 21].

In order to characterize the resulting crystals, we use a Leika stereoscan 440 scanning electron microscope (SEM) equipped with EDX/WDX, and a Siemens D-500 x-ray powder diffractometer with Cu Kα radiation. Both were used to perform local elemental analysis and phase identification, respectively. The single crystals were studied at room temperature using a Siemens P4 diffractometer with a monochromatized Mo Kα radiation ($\lambda = 0.710\,73$ Å, 1.5 kW). The cell parameters were refined using a large set (90–99) of centered reflections and a complete Ewald sphere (eight octant) was measured [22] for each crystal up to $2\theta = 90^\circ$ with $\theta/2\theta$ scans and a variable scan speed. No corrections were applied for high-angle reflections for which diffraction peaks for Mo Kα_I and Mo Kα_{II} are separated. Because of the very high absorption coefficients it was essential to correct data for this effect. ψ-scans with χ close to 90° were measured and the correction was applied considering the crystals to be laminar [22]. Structures were refined by standard full matrix least-squares cycles [23]. Extinction corrections were systematically applied, and an appropriate weighing scheme employed in the last cycles. Pertinent data are reported in table 1, while complete results are available from the deposited CIF file.

Resistivity as a function of temperature was measured using a dc four-probe technique in a PPMS 6000 Quantum Design system. Four 25 μm gold wires were attached to the sample using silver paint. Dc magnetization was measured from 2 to 300 K using a (SQUID) magnetometer.
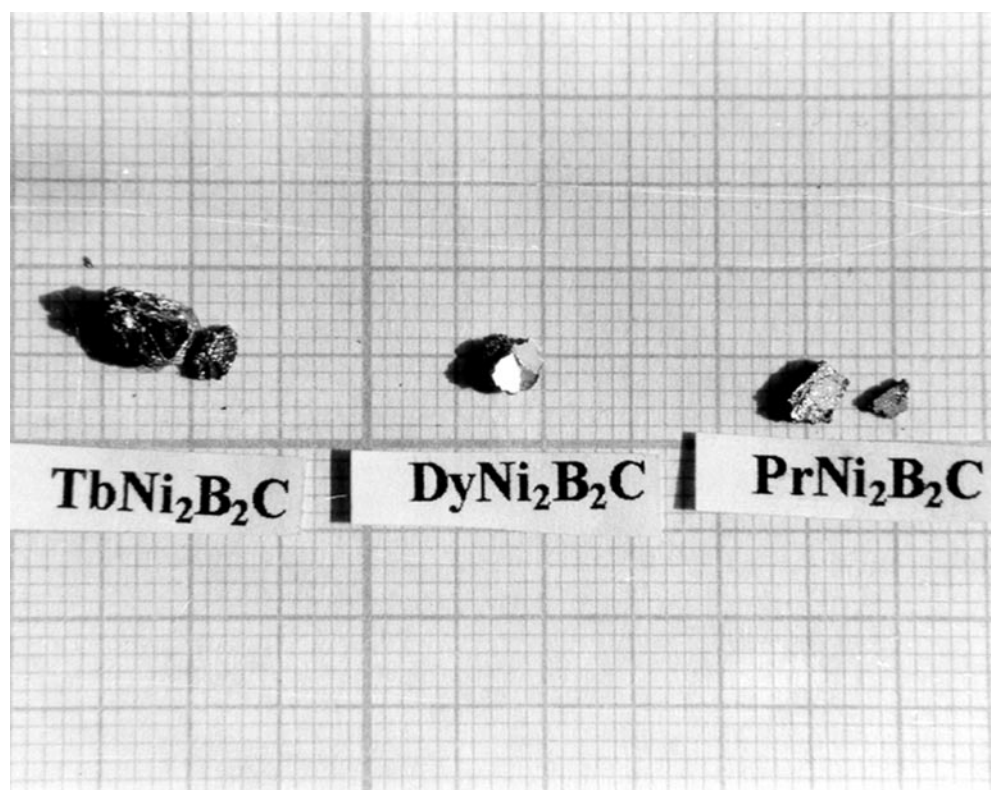
Figure 1. As-grown button of PrNi$_2$B$_2$C, DyNi$_2$B$_2$C, and TbNi$_2$B$_2$C. Well defined flat facets can clearly be observed. The facets are related to the {002} family of planes.

## 3. Results and discussion

3.1. Crystal characterization

The x-ray diffraction patterns of the polycrystalline phase display mainly reflections of RB$_2$C$_2$ ($2\theta = 23.2°$), and RNi$_4$B ($2\theta = 44.6°$) and weak reflections of Ni$_3$B ($2\theta = 53.2°$). The crystallization of the melts is in agreement with earlier work [16]. Behr *et al* [11, 17] employing a floating-zone technique in the RNi$_2$B$_2$C system show that properitectic RB$_2$C$_2$ phase is the primary phase from which RNi$_2$B$_2$C is formed by peritectic reaction; the solidification process ends with RNi$_4$B and Ni$_3$B phases. The single crystals result from the undercooled melt of the peritectic reaction. In figure 1 we show samples of polycrystalline as-grown bulk; well defined flat facets are clearly observed. Structural studies reveal that the flat facets in the crystal habit are related to the family of {002} planes. WDX analysis was used because of its high sensitivity for light elements such as boron and carbon. Typical analysis for a single crystal of HoNi$_2$B$_2$C shows: 54.93 wt% Ho, 37.98 wt% Ni, 3.07 wt% B and 4.29 wt% C, indicating that the phase can be correctly identified with stoichiometry 1:2:2:1, without any detected second phase.

For each single crystal the *I* Bravais mode and the 4/*mmm* Laue group were confirmed from rotation photographs and by measuring the symmetric equivalent intensities. Photographic studies revealed the single-crystal nature of the samples (no extra spots were observed). The mosaic spread of the single crystals was monitored using the strong (004)
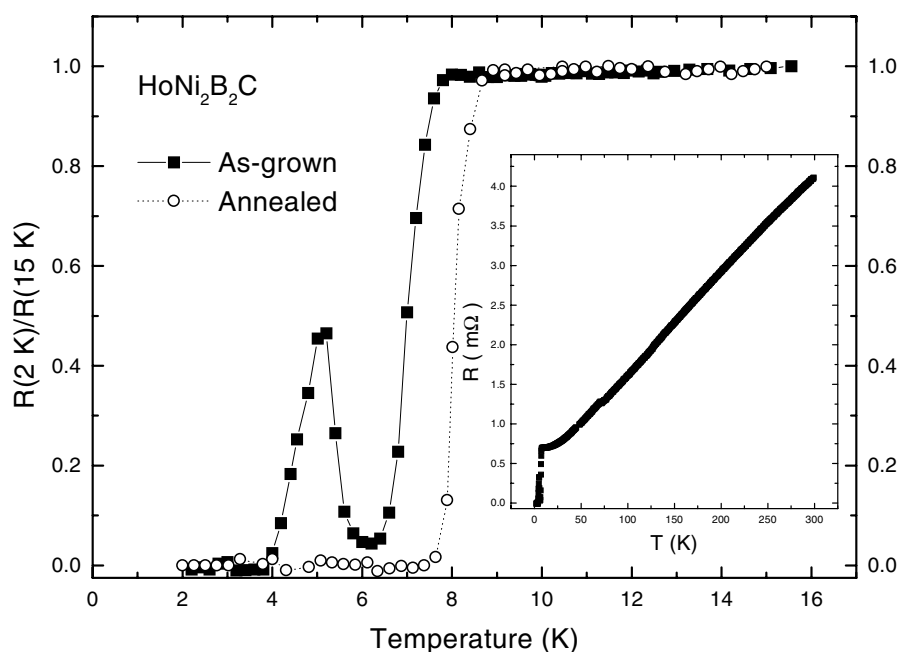
Figure 2. Temperature dependence of the in-plane resistivity for HoNi$_2$B$_2$C single crystals as-grown (closed squares) and annealed (open circles) for 5 days (at 1050 °C) near T_c. The inset shows resistivity versus temperature from room temperature to 2 K.

reflection. The full width at half maximum (FWHM) spans a small range from 0.30(1)° (Tb, Pr) to 0.32(1)° (Dy, Pr), indicating that the reported method for crystal growth achieves a reproducible mosaicity, regardless of the nature of the rare earth. Furthermore, it should be mentioned that in the case of an annealed TbNi$_2$B$_2$C a very similar FWHM of 0.31(1)° was measured for the same reflection. Crystal quality is also manifested in the fact that no reflections with $I < 2\sigma(I)$ were observed. As expected, the cell volume decreases from R = Pr to R = Ho in accordance with the ionic radius. The variations of the parameters of the tetragonal cell and its volume are presented in table 1. All compounds are isostructural to that previously reported for R = Lu [6, 7]. However, due to changes in the c/a ratio, from 2.70 for R = Pr to 3.00 for R = Ho, significant variations in the geometry can be observed. For the rare-earth carbide layers normal to the c axis, the R–C separation decreases drastically from 2.6160(1) Å for R = Pr to 2.4826(1) Å for R = Ho. A similar variation is observed for the Ni$_2$B$_2$ layers intercalated between the R–C sheets. For example, the Ni–B distance ranges from 2.109(2) to 2.102(4) Å. The elongation of the cell along the c axis is also reflected in angles within the Ni$_2$B$_2$ layers. For instance, the angle Ni–B–Ni significantly varies from 76.67(7)° (R = Pr) to 72.4(1)° (R = Ho). As a general view, incrementing the c/a ratio by substitution of a heavier rare earth yields a separation of the sheets in the layered structure, and a shortening of contacts between atoms, within the sheets. A remarkable confirmation of this behaviour can be inferred from a comparison of the thermal parameters. For all atoms, thermal motions depicted by the U_{iso} parameters are lower for R = Ho than for R = Pr, mainly because the density of atoms in the layers normal to the c axis increases from Pr to Ho. Indirectly, this observation also indicates that inter-layer contacts are weak compared to those within the layers.
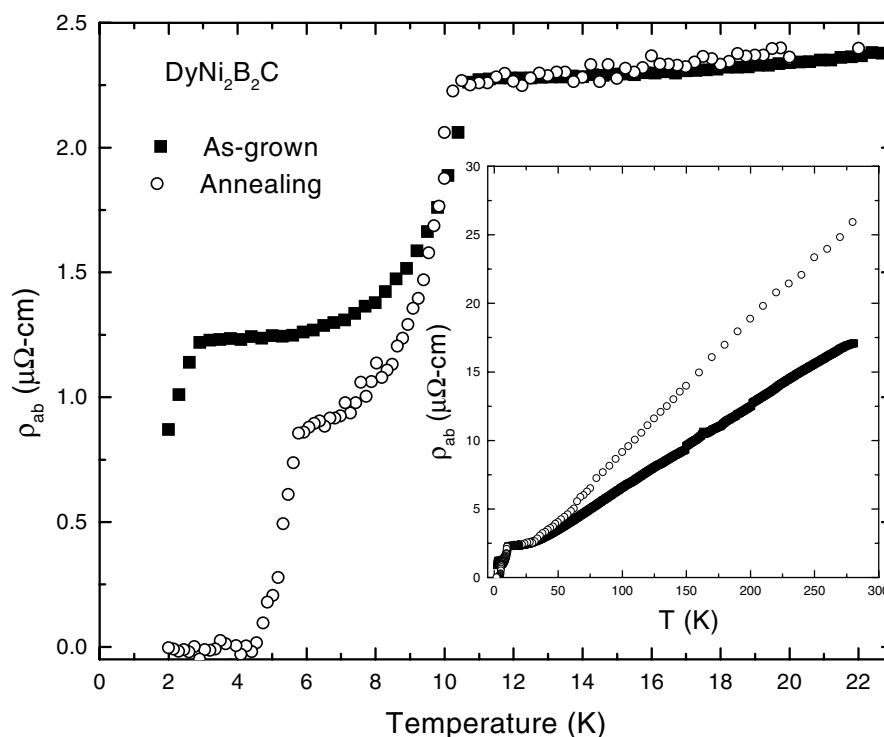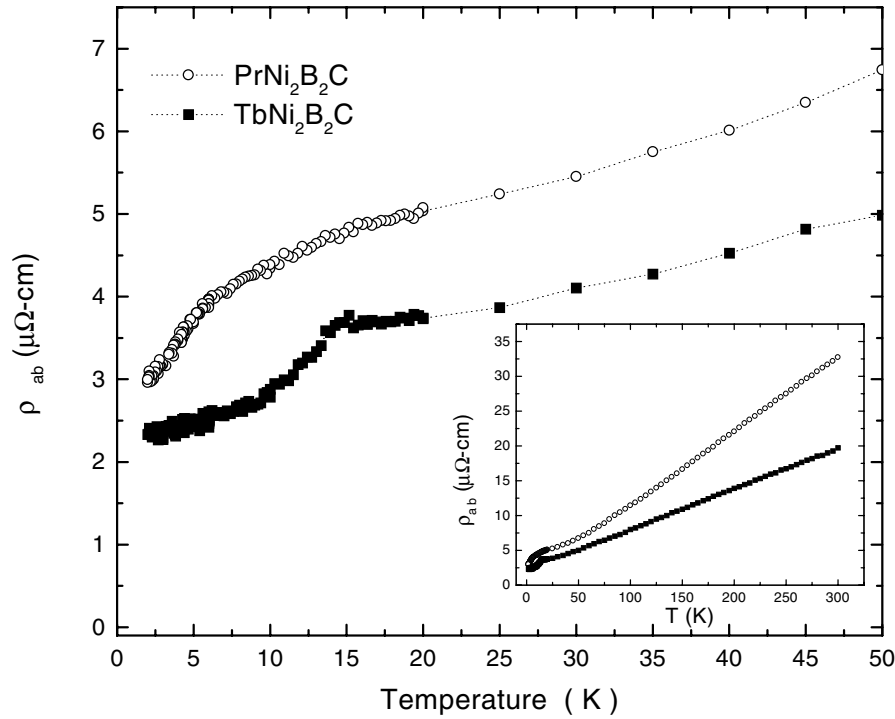
Figure 3. Temperature dependence of the in-plane resistivity of an as-grown DyNi$_2$B$_2$C single crystal (closed squares), and the result of annealing for 5 days at a temperature of about 1050 °C (open circles). The inset shows the characteristic resistivity versus temperature.

3.2. Resistivity measurements

The results of in-plane resistivity (ρ) measurements of RNi$_2$B$_2$C (R = Ho, Dy, Tb and Pr) are shown in figures 2–4. For the HoNi$_2$B$_2$C single crystal of figure 2 we show the R–T characteristic taken at low temperature for the as-grown and annealed samples. The onset of the superconducting transition is at 7.6 K for the as-grown sample. As the temperature is decreased a reentrant behaviour to the normal state occurs at 5.6 K, with a maximum in resistance at 5.2 K. This maximum only reaches about 50% of the value of the resistance at 7.8 K, after which the resistance decreases again, and vanishes at 4.4 K. The reentrant behaviour without applied magnetic field for as-grown single crystal is observed in the region where neutron scattering indicates a modulated magnetic structure [24, 25]. We must remember that this reentrant behaviour was not observed in general in single crystals grown by flux method [26, 27], where crystals are grown by flux methods. In this case one could argue that in fact a percolative path for the supercurrent exists between magnetic domains and superconducting islands, and is similar to that observed in other magnetic superconductors [28, 29]. We observe a sample annealed for 5 days in the same figure; the reentrant behaviour disappears and the onset of the superconducting transition increases at about 8.5 K.

In figure 3, we show resistivity versus temperature data for a DyNi$_2$B$_2$C single crystal. First of all, we note a steep decrease at about 10.5 K, which is the signature of the antiferromagnetic Néel temperature, T_N. The value of T_N agrees well with similar observations by others workers in polycrystalline and single crystal samples [19, 30, 31]. In our as-grown crystals

Figure 4. Temperature dependence of the in-plane resistivity of as-grown PrNi$_2$B$_2$C (open circles) and TbNi$_2$B$_2$C (closed squares) single crystals. The inset shows the characteristic resistivity versus temperature from room temperature to low temperature.

the superconducting temperature is below 2 K, but after annealing the transition temperature increases to about 4.8 K with a width of the transition of the order of $\Delta T \sim 0.8$ K. This suggests a close connection between crystallinity (class of disorder, superficial defects, internal stress) and electronic properties mainly for Ho2:2:1 and Dy2:2:1 compounds, respectively, as we discuss at the end of this section.

In figure 4, we have plotted the in-plane resistivity for two single crystals, one of PrNi$_2$B$_2$C and the other of TbNi$_2$B$_2$C. They did not show superconductivity at the minimum attainable temperatures of 2 K for the Tb2:2:1 compound, nor for the Pr2:2:1 compound when measured at about 0.3 K. The room temperature resistivities for both compounds were 33 $\mu\Omega$ cm, and 20 $\mu\Omega$ cm for the Pr2:2:1 and Tb2:2:1 compounds, respectively. At low temperature, for the Tb-based compounds the antiferromagnetic (AF) transition T_N at about 15 K can clearly be seen. This extra scattering is noted as a sharp change in the slope of the resistivity versus temperature curve. This should be compared with the smooth feature, in the same figure, for PrNi$_2$B$_2$C at about 4 K. The Néel transition in the Tb-based compound coincides with previously published data [32]. We no observed considerable effects in as-grown and annealed samples for these two last compounds.

It is important to mention that our resistivity measurements in these single crystals correspond well with values observed by other workers. However, some differences were found by different workers; for the Ho-based compound Cimberle *et al* [33] report resistivities of the order of 42 $\mu\Omega$ cm at 12 K in polycrystalline samples, and Schmidt *et al* [34] have shown several superconducting–reentrant–superconducting transitions in polycrystalline samples,
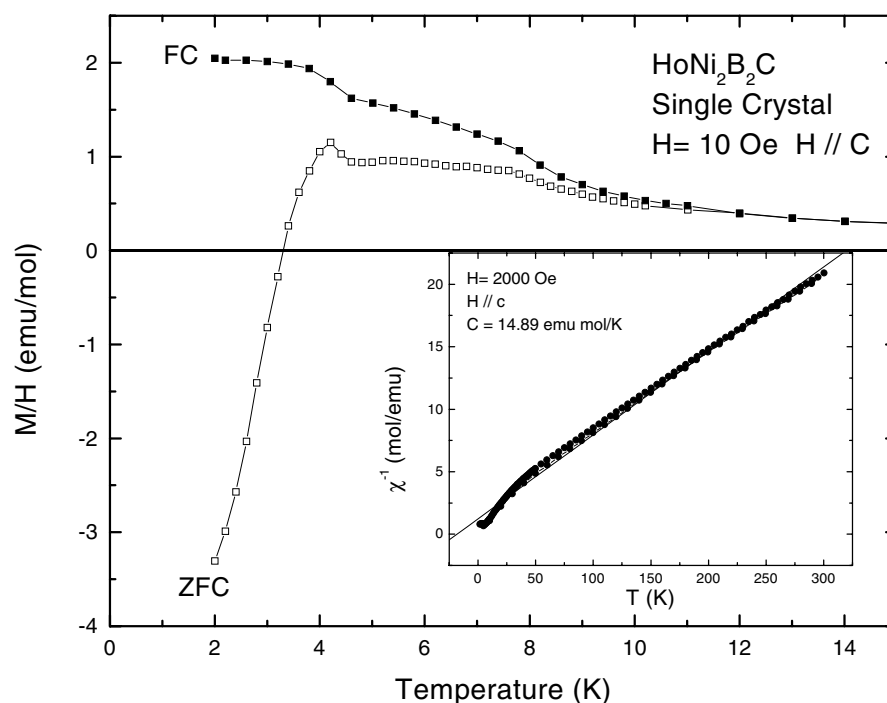
Figure 5. Zero-field cooling (ZFC) and field cooling (FC) susceptibility measurements for HoNi$_2$B$_2$C in an applied field of 10 Oe. The inset shows $1/\chi$ versus T measured in the presence of a field of 2000 Oe, both measurements being performed with the field parallel to the *c*-axis.

arguing that these resistivity values depend strongly on the stoichiometry and the thermal treatment. Nevertheless, there is a large difference for single crystals where resistivity ratios of about 10–11 have been found, and values of resistivities (close to T_c) of the order of 4–8 $\mu\Omega$ cm and non-reentrant behaviour without applied field [26, 27]. Tomy *et al* [19] show that the superconductivity of DyNi$_2$B$_2$C is very sensitive to the stoichiometric composition of mainly carbon. In particular, our samples show that the superconducting phase depends on homogenization, relaxing stress and the redistribution of boron and carbon. Such conclusions were reached after long annealing times in our as-grown crystals. To substantiate this claim, in figures 2 and 3 we show in the change in superconducting behaviour after as-grown crystals were annealed for 5 days at 1100 °C. The superconducting transitions appear at ∼8.0 and ∼4.4 K and the resistivity ratio increases from 6.5 to 10 and 14 to 21 for HoNi$_2$B$_2$C and DyNi$_2$B$_2$C, respectively. It is interesting to mention that in single crystals the reentrant behaviour is not a common feature. It was observed in our single crystals, and by Fisher *et al* [35]. They mention that only in some of their crystals does the reentrance appear; they attribute this effect to strains created when cutting or polishing the crystals. In our cold crucible crystals we observed reentrance in all of them; it disappears once they are annealed. We associated this with the internal stresses produced during the growth steps. Once annealed they are released. However, it is important to note that in polycrystalline samples the annealing does not cause reentrance to disappear, as was demonstrated by Wagner *et al* [36]. As in other crystals, in DyNi$_2$B$_2$C grown by the cold crucible method, annealing improves the electronic properties, but until now they appear with lower superconducting temperature than others grown by the flux method. We are studying this problem. Nevertheless, it is not just
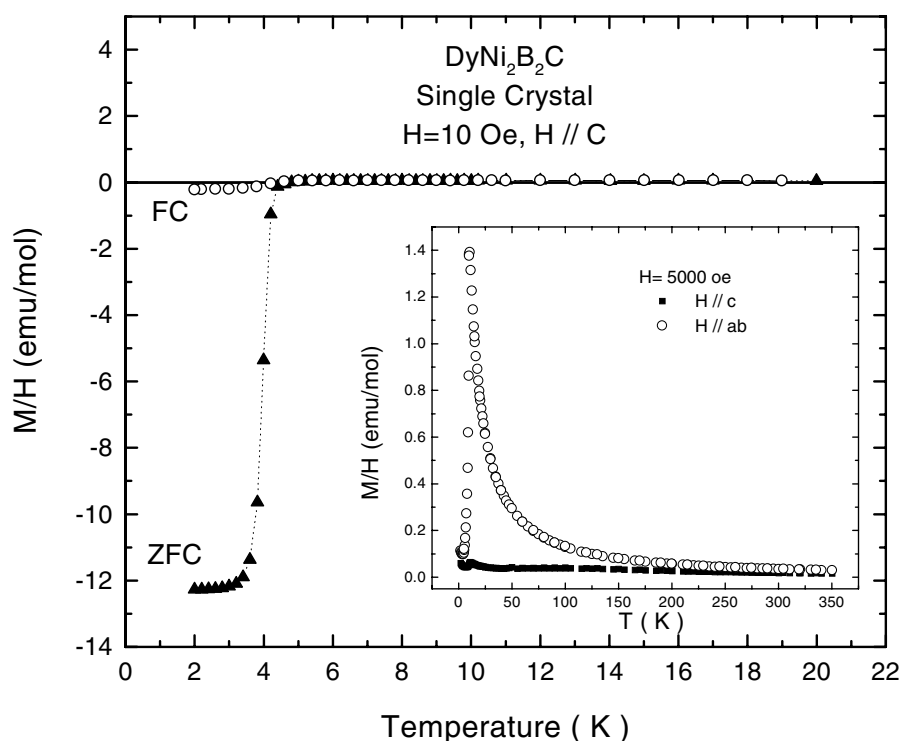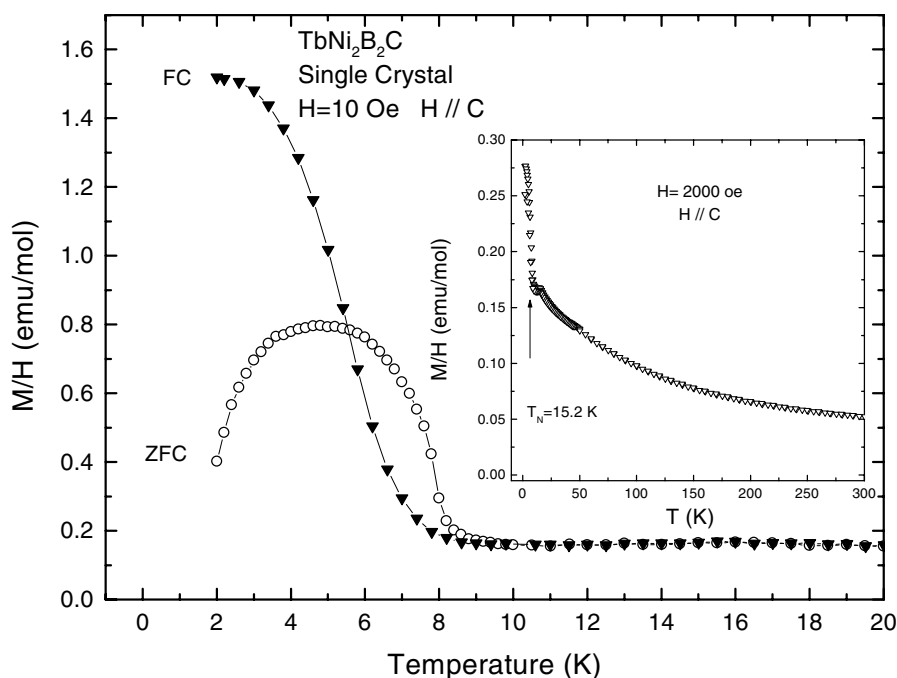
Figure 6. Zero-field cooling (ZFC) and field cooling (FC) susceptibility measurements for DyNi$_2$B$_2$C in an applied field of 10 Oe parallel to the *c*-axis. The inset shows the magnetic susceptibility in a field of 5000 Oe parallel for both directions.

the annealing that is responsible for the electronic characteristics of this compound, but a combination of the correct stoichiometry of boron and carbon and the annealing conditions. It is worth emphasizing that homogenization or redistribution in the cell of light elements (B and C) is a normal process occurring whenever metals or alloys are annealed, so that redistribution of elements results from the annealing being performed at high temperatures (∼1050 °C) for long periods of time. Secondly, for light atoms the rate of diffusion is high, therefore increasing the ion mobility to the corresponding cell sites.

3.3. Magnetic measurements

The temperature dependence of the magnetic susceptibility of HoNi$_2$B$_2$C in one of the as-grown single-crystal samples is shown in figure 5. Applied fields were 10 and 2000 Oe along the *c*-axis direction. The inset shows a plot of $1/\chi$ against T, and seems to follow a Curie–Weiss law with an effective moment of the order of $\mu_{eff} = 10.88 \, \mu_B$, and a paramagnetic Curie temperature of $\Theta = -6.6$ K. This value of μ_{eff} is very close to the effective moment of the free Ho^{3+} ion (10.60 μ_B) [37, 38]. In the temperature range between 8 and 5 K in the zero-field cooling measurement mode (ZFC) we observe a plateau. This has been seen also in polycrystals with different carbon stoichiometries and in samples treated under different thermal process [34]. This is indicative of different scattering processes occurring in the compound. In the reentrant region neutron diffraction studies [24, 25] show several incommensurate spiral magnetic states; these modulated states disrupt superconductivity through the increase of pair breaking. At the

Figure 7. Zero-field cooling (ZFC) and field cooling (FC) susceptibility for TbNi$_2$B$_2$C measured in a field of 10 Oe parallel to the *c*-axis. The inset shows the susceptibility measured in the field of 2000 Oe. Note the feature in T_N at about 15 K.

Néel temperature ($T_N \sim 5$ K) they collapse in favour of a simple antiferromagnetic state which coexists with superconductivity. Thus, in this small range of temperatures magnetic domains coexist with superconducting islands. In this temperature range only percolative paths allow the resulting resistance of the measured sample to be zero. As the temperature is lowered the competition of the two processes produces an interesting balance between magnetism and superconductivity. Magnetic domains grow in size and enclose more volume of the sample. However, at the same time the superconducting condensate is reinforced. As a consequence this competition cause the percolative path for the electrical current to open or close in such a way that the resistance of the sample is zero or nonzero. This is perhaps a way of explaining why other workers sometimes find or do not find reentrant behaviour in this compound.

In order to study the magnetic properties of our DyNi$_2$B$_2$C single crystal, magnetic susceptibility measurements in ZFC and FC modes at 10 Oe were performed. We display these measurements in figure 6. In ZFC a sharp transition to the superconducting state is seen at about 4.2 K. In the inset the value of the susceptibility measured at a field of 5000 Oe along both the *a*–*b*-axis and *c*-axis directions is shown. Along the *a*–*b*-axis the effective moment is about $\mu_{eff} = 10.86\ \mu_B$, with Curie–Weiss temperature $\Theta = -0.0148$ K. This effective moment is very close to the theoretical value of 10.63 μ_B for the free Dy^{3+} ion. However, in the *c*-axis direction μ_{eff} was found to be only 6.75 μ_B with $\Theta = 0.000\,84$ K, this low value revealing a weak paramagnetic contribution from the Dy sublattice in that plane. However the measured flux expulsion at 2 K was only about 4% of the ideal value $H/4\pi$ and the shielding fraction was about 200%. These values are larger that the previously reported by Lin *et al* [39] in polycrystalline samples, but slightly smaller than reported by Cho *et al* [30] for single crystals.
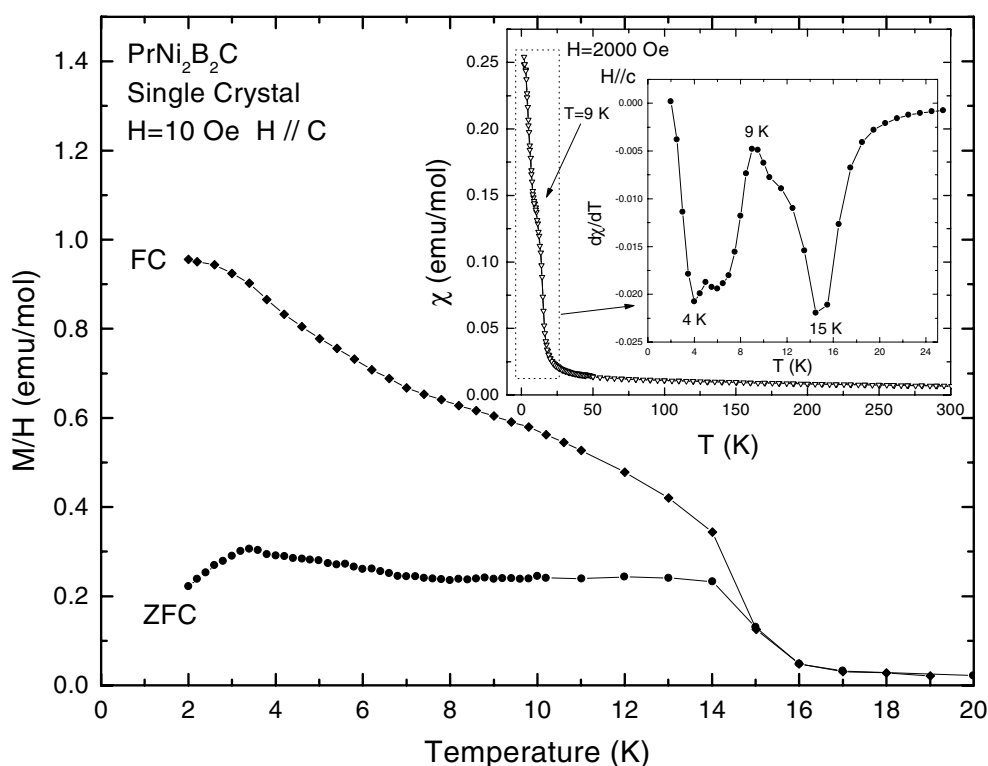
Figure 8. Zero-field cooling (ZFC) and field cooling (FC) susceptibility for a PrNi$_2$B$_2$C single crystals measured in a field of 10 Oe parallel to the c-axis. The inset shows the susceptibility measured in a field of 2000 Oe, and the temperature derivative of the susceptibility as a function of temperature. Peaks appear at 15, 9 and 4 K, indicating different magnetic interactions.

Low- and high-field susceptibilities for TbNi$_2$B$_2$C and PrNi$_2$B$_2$C single crystals are shown in figures 7 and 8. Both figures clearly suggest the presence of magnetic anomalies. Figure 7 shows the presence of two magnetic transitions, one at about 8 K (see inset) and another at about 15.2 K. The first transition corresponds to the magnetic ordering of the Tb atoms, which has been confirmed by neutron measurements [40]. The second transition is of antiferromagnetic character, and occurs at about 15.2 K [41]. Magnetic studies carried out by Cho *et al* [32] attribute the second transition to the emergence of a weak ferromagnetic ordering (WFM), which appears at 9 K and saturates at 5 K in ZFC measurements. Curie–Weiss fitting leads to $\mu_{eff} = 10.79\,\mu_B$ and $\Theta = -64.49$ K. This value of μ_{eff} is about 1 μ_B higher than the free Tb^{3+} ion value of 9.72 μ_B. In figure 8 we show susceptibility measurements performed in ZFC and FC modes for one of our single crystals of PrNi$_2$B$_2$C composition. We noted for this single crystal, as in other rare earth compounds of this family, that the magnetic behaviour is rather complicated and shows many magnetic features at different temperatures. For instance, in the ZFC and FC measurements different anomalies can be observed. At about 16 K, the ZFC and FC separate into two curves. At lower temperature the separation is larger and other features can be seen; for instance at about 3.5 K a small maximum is clearly observed in the ZFC mode while in FC this feature shows up only as a change in curvature. The inset of this figure shows dχ/dT, where three anomalies at 4, 9 and 15 K can be noted. At least two of these transitions have been observed in polycrystalline samples by Lynn *et al* [42] and by Takeya *et al* [43].
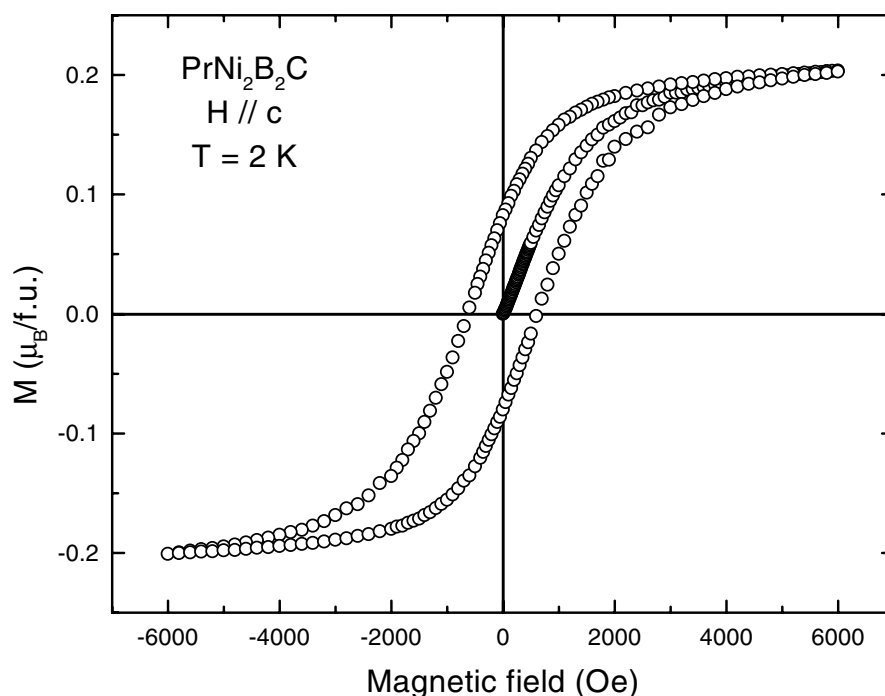
Figure 9. Ferromagnetic behaviour observed in magnetization *M* versus magnetic field curves for a PrNi$_2$B$_2$C single crystal at 2 K for *H* ∥ *c*-axis.

Both confirm that these transitions are of AF nature (at 4 and 15 K). The resulting fitted values from the Curie–Weiss law for powered crystals gave; $\mu_{eff} = 3.53 \ \mu_B$ and $\Theta = -0.014$ K. Takeya *et al* [43] reported $\mu_{eff} = 3.46 \ \mu_B$, being close to the theoretical value of 3.58 μ_B for the free Pr^{3+} ion. Features similar to ours are also reported in their low-field magnetization measurements. But it is worthwhile mentioning that the anomaly at $T = 9$ K in high field was not reported in their studies.

In order to understand more about the magnetic nature of the compound we performed isothermal measurements of the magnetization versus magnetic field at 2 K, along the *c*-axis direction. Figure 9 shows that indeed ferromagnetic behaviour may be the reason for the absence of superconductivity in this compound. The data show large hysteresis for a complete field cycle. The saturation moment is only about 0.2 μ_B fu^{-1}, which is quite low compared with that of the Pr^{3+} free ion, but very characteristic of heavy-fermion systems. This value is close to that reported by Lynn *et al* [43]. One final issue to investigate in the PrNi$_2$B$_2$C system is whether this ferromagnetic state is responsible for the lack of the superconducting behaviour.

4. Conclusions

We have presented some physical characteristics of RNi$_2$B$_2$C (R = Ho, Dy, Tb, Pr) single crystals grown by using a cold copper crucible technique. Our single crystals were completely characterized in composition and structure determinations were refined by standard full-matrix least-square cycles. X-ray studies did not detect second phases. Single crystal growth of

RNi$_2$B$_2$C (R = Ho, Dy, Tb and Pr) intermetallic alloys was performed without any solvent. In general magnetic and transport studies show similar behaviour as previously published on single-crystal and polycrystalline growth by other methods. For DyNi$_2$B$_2$C we found the superconducting transition at about 4.8 K. In the TbNi$_2$B$_2$C single crystals we did not observe any difference between single crystals grown by the flux method or by the cold-copper crucible technique. A very interesting observation found in our PrNi$_2$B$_2$C single crystals is the ferromagnetic ordering measured at low temperature, which is reasonable to assume to explain the absence of superconductivity. Finally, we believe the cold copper crucible method to be a useful alternative technique for the growth of single crystals of this borocarbide family.

Acknowledgments

References

[1] Mazumdar C, Nagarajan R, Godart C, Gupta L C, Latroche M, Dhar S K, Levy-Clement C, Padalia B D and Vijayaraghavan R 1993 *Solid State Commun.* **87** 413–16
[2] Eisaki H, Takagi H, Cava R J, Batlogg B, Krajewski J J, Peck W F, Mizuhashi K, Lee J O and Uchida S 1994 *Phys. Rev.* B **50** 647–50
[3] Cava R J *et al* 1994 *Nature* **367** 252–3
[4] Ferting W A, Johnston D C, DeLong L E, McCalum R W, Maple M B and Matthias B T 1977 *Phys. Rev. Lett.* **38** 987–90
   Sinha S K, Crabtree G W. Hinks D G and Mook H 1982 *Phys. Rev. Lett.* **48** 950–3
   Behroozi F, Hall L N, Crabtree G W and Hink D G 1989 *Phys. Rev.* B **40** 6548–57
[5] Maple M B 1995 *Physica* B **215** 110–26
[6] Siegrist T, Zandbergen H W, Cava R J, Krajewski J J and Peck W F Jr 1994 *Nature* **367** 254–6
[7] Siegrist T, Cava R J, Krajewski J J and Peck W F Jr 1994 *J. Alloys Compounds* **216** 135–9
[8] Lai C C, Lin M S, You Y B and Ku H C 1994 *Phys. Rev.* B **50** 620–3
[9] Jeng F S, You Y B, Ku H C and Ho J C 1996 *Phys. Rev.* B **53** 3492–6
[10] Cava R J *et al* 1994 *Nature* **367** 146–8
[11] Behr G, Löser W, Graw G and Nenkov K 1999 *J. Mater. Res.* **14** 16–23
[12] Canfield P C, Gammel P L and Bishop D J 1998 *Phys. Today* October 40–6
[13] Xu M, Canfield P C, Ostenson J E, Finnemore D K, Cho B K, Wang Z R and Johnston D C 1994 *Physica* C **227** 321–6
[14] Cho B K, Canfield P C, Miller L L, Johnston D C, Beyermann W P and Yatskar A 1995 *Phys. Rev.* B **52** 3684–95
[15] Cho B K, Xu M, Canfield P C, Miller L L, Johnston D C, Beyermann W P and Yatskar A 1995 *Phys. Rev.* B **52** 3676–83
[16] Takeya H, Kadowaki K, Mirata K and Mirano T 1996 *Physica* C **256** 220–6
[17] Behr G, Loser W, Graw G, Bitterlich H, Freudenberger J, Fink J and Schultz L 1999 *J. Cryst. Growth* **198/199** 642–8
[18] Schmidt H, Weber M and Braun H F 1995 *Physica* C **246** 177–85
[19] Tomy C V, Balakrishnan G and Paul McK D 1995 *Physica* C **248** 349–52
[20] Aleksandrov V I, Osiko V V, Prokhorov A M and Tatarintsev V M 1978 *Current Topics Mater. Sci.* **1** 428–81
[21] Christensen A N 1983 *J. Cryst. Growth* **62** 320–8
[22] Fait J 1991 *SCANS* (Madison, WI: Siemens)
[23] Sheldrick G M 1997 *SHElX97 Users Manual* University of Göttingen
[24] Huang Q, Santoro A, Grigert T E, Lynn J W, Cava R J, Krajewski J J and Peck W F Jr 1995 *Phys. Rev.* B 51 3701–8
[25] Grigereit T E, Lynn J W, Huang Q, Santoro A, Cava R J, Krajewski J J and Peck W F Jr 1994 *Phys. Rev. Lett.* **73** 2756–9

[26] Rathnayaka K D D, Naugle D G, Cho B K and Canfield P C 1996 *Phys. Rev.* B **53** 5688–95
[27] Bhatnagar A K, Rathnayaka K D D, Naugle D G and Canfield P C 1997 *Phys. Rev.* B **56** 437–45
[28] Bulaevskii B L, Buzdin A I, Kulic M L, Panjukov S V, 1985 *Adv. Phys.* **4** 175–81
     Burlet P, Flouquet J, Genicon J L, Horyn R, Peña O and Sergent M 1995 *Physica* B **215** 127–33
[29] Morales F, Escudero R, Briggs A, Monceau P, Horyn R, Le Berre F and Peña O 1996 *Physica* B **218** 193–6
[30] Cho B K, Canfield P C and Johnston D C 1997 *Phys. Rev.* B 52 R3844–7
[31] Peng Z Q, Krug K and Winzer K 1998 *Phys. Rev.* B 57 R8123–6
[32] Cho B K, Canfield P C and Johnston D C 1995 *Phys. Rev.* B 53 8499–508
[33] Cimberle M R *et al* 1996 *Solid State Commun.* **99** 209–14
[34] Schmidt H, Dertinger A, Ernstberger B and Braun H F 1997 *J. Alloys Compounds* **262–263** 459–61
[35] Fisher I R, Cooper J R and Canfield P C 1997 *Phys. Rev.* B **56** 10 820–3
[36] Wagner T A, Dertinger A, Ettig W, Krause A, Schmidt H and Braun H F 1999 *Physica* C **323** 71–8
[37] Cho B K, Harmon B N, Johnston D C and Canfield P C 1996 *Phys. Rev.* B **53** 2217–20
[38] Canfield P C, Cho B K, Johnston D C, Finnemore D K and Hundley 1996 *Physica* C **267** 397–406
[39] Lin M S, Shieh J H, You Y B, Hsu Y Y, Chen J W, Lin S H, Yao Y D, Chen Y Y, Ho J C and Ku H C 1995
     Physica C **249** 403–8
[40] Dervenegas P, Zarestky J, Stassis C, Goldman A I, Canfield P C and Cho B K 1996 *Phys. Rev.* B **53** 8499–508
[41] Tomy C V, Afalfiz L A, Lees M R, Martin J M, Paul M and Adroja D T 1996 *Phys. Rev.* B **53** 307–12
[42] Lynn J W, Skanthakumar S, Huang Q, Santoro A, Sinha S K, Hossain Z Z, Gupta L C, Nagarajan R and Godart C
     1997 *Phys. Rev.* B **55** 6584–98
[43] Takeya H and Kuznietz M 1999 *J. Magn. Magn. Mater.* **195** 366–75